

Annihilation of photo induced minority carrier caused by ion implantation and rapid thermal annealing

Toshiyuki Sameshima^{1*} and Satoshi Shibata²

¹Tokyo University of Agriculture and Technology, Koganei, Tokyo 184-8588, Japan

²Panasonic Corporation, Moriguchi, Osaka 570-8501, Japan

E-mail: tsamesim@cc.tuat.ac.jp

Received December 10, 2013; revised January 26, 2014; accepted February 23, 2014; published online April 30, 2014

We report decreases in the minority carrier effective lifetime τ_{eff} of 700- μm -thick silicon substrates coated with 43-nm-thick thermally grown SiO_2 layers by Ge ion implantation with a dose of $1 \times 10^{13} \text{ cm}^{-2}$ at 150 keV and rapid thermal annealing (RTA) at 1100 °C for 50 s. Ge ion implantation decreased the crystalline volume ratio in the top 157 nm region because of lattice damage. It also markedly decreased τ_{eff} to 1.6×10^{-6} and 9.5×10^{-6} s when 635 and 980 nm lights were continuously illuminated to the implanted surface, respectively. Small τ_{eff} values resulted from serious damage with a high surface recombination velocity S of 2.0×10^4 cm/s and a short bulk lifetime of 5.0×10^{-6} s in the 200 μm deep surface region. Although RTA successfully recrystallized the Ge-implanted surface region, it further decreased τ_{eff} to 1.1×10^{-6} and 2.2×10^{-6} s in the cases of 635 and 980 nm light illuminations to the top surfaces, respectively. RTA caused a high density of recombination sites with a high S value of 3.0×10^4 cm/s on the top and rear surfaces. There was a high density of interface traps of $9.1 \times 10^{11} \text{ eV}^{-1} \text{ cm}^{-2}$. 1.3×10^6 Pa H_2O vapor heat treatment at 260 °C for 3 h markedly increased τ_{eff} to 6.5×10^{-4} and 6.9×10^{-4} s in the cases of 635 and 980 nm light illuminations. The interface trap density was decreased to $3.6 \times 10^{10} \text{ eV}^{-1} \text{ cm}^{-2}$. Low temperature post annealing is effective in curing the recombination defect states induced by RTA. © 2014 The Japan Society of Applied Physics

1. Introduction

Ion implantation and rapid thermal annealing (RTA) are important methods for the current fabrication technology of silicon large-scale integrated circuits.^{1–4} RTA makes it possible to heat samples at a high temperature of around 1100 °C for short times less than 1 min. RTA induces the activation of implanted dopant atoms by substantially suppressing the diffusion of dopant atoms in silicon. Moreover, it cures the crystalline state well, which was once deteriorated by high-energy ion irradiation during implantation. The pn junction is successfully formed by ion implantation and subsequent RTA. It is the fundamental structure for fabricating metal–oxide–semiconductor field-effect transistors, bipolar transistors, photosensors,^{5–9} and solar cells.^{10–13} We have recently reported that the minority carrier effective lifetime τ_{eff} markedly decreased when silicon substrates were rapidly heated to a high temperature by an infrared laser.¹⁴ A decrease in τ_{eff} indicates that a substantial number of minority carrier recombination defect states is generated during heating. It is a serious problem to be solved in fabricating photosensors and solar cell devices.

In this paper, we report an investigation of annihilation properties of photo induced carriers in the cases of germanium (Ge) ion implantation and RTA for silicon substrates. Ge is a group IV element, which does not form a carrier in silicon and a built-in potential. It is suitable for investigating defects induced by ion implantation and RTA. We used a highly sensitive measurement system for τ_{eff} using the microwave absorption caused by photo induced free carriers under light illumination at two different wavelengths of 635 and 980 nm.¹⁵ We report that Ge ion implantation generated carrier recombination defects in deep regions as well as in surface regions. We also report that RTA also generated carrier recombination defects in surface regions. We suggest that a postannealing process will be important in curing defective states induced by RTA.

Table I. Sample description.

Sample	Processes
<i>A</i>	as is
<i>B</i>	Ge implantation at dose of $1 \times 10^{13} \text{ cm}^{-2}$ at 150 keV
<i>C</i>	Ge implantation + RTA at 1100 °C for 50 s
<i>D</i>	RTA
<i>B</i> _{anneal}	Ge implantation + 1.3×10^6 Pa H_2O vapor heat treatment at 260 °C for 3 h
<i>C</i> _{anneal}	Ge implantation + RTA + H_2O vapor heat treatment
<i>D</i> _{anneal}	RTA + H_2O vapor heat treatment

2. Experimental procedure

13 $\Omega \text{ cm}$ p-type silicon substrates with a thickness of 700 μm , a diameter of 8 in., and a crystalline orientation of (100) were prepared. The substrates were coated with 43-nm-thick thermally grown SiO_2 layers by heating in dry oxygen atmosphere at 1100 °C for surface passivation. The substrates were cut to four pieces named *A*, *B*, *C*, and *D*, as shown in Table I. Ge ion implantation was carried out at a dose of $1 \times 10^{13} \text{ cm}^{-2}$ at 150 keV in samples *B* and *C*. The analysis with a numerical calculation program of stopping and range of ions in matter (SRIM)¹⁶ revealed that the Ge concentration had a peak concentration of $1.4 \times 10^{18} \text{ cm}^{-3}$ at 84 nm from the top SiO_2 surface (41 nm from the silicon surface). In the silicon substrate, 99% of the Ge atoms concentrated within 125 nm from the silicon surface. Samples *C* and *D* were heated by RTA in N_2 atmosphere at 1100 °C for 50 s. Sample *A* was therefore a control sample.

Heat treatment with 1.3×10^6 Pa H_2O vapor at 260 °C for 3 h was subsequently applied to samples *B*, *C*, and *D* as low-temperature post annealing for defect reduction.^{17–20} H_2O -vapor-annealed samples were named *B*_{anneal}, *C*_{anneal}, and *D*_{anneal}, as shown in Table I.

To measure τ_{eff} precisely, we used a 9.35-GHz-microwave-transmittance measurement system, as shown by a schematic in Fig. 1.^{15,21,22} The system had waveguide tubes, which had

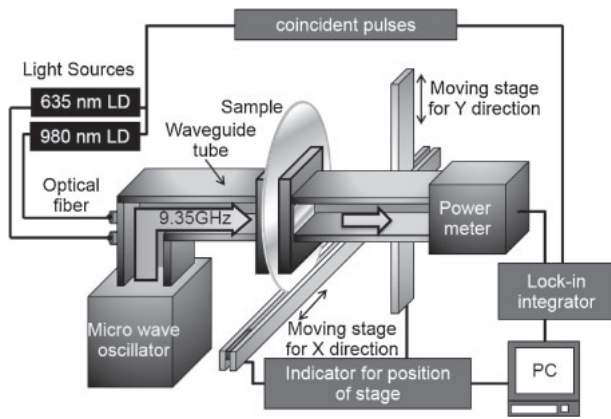


Fig. 1. Schematic photoinduced carrier microwave absorption measurement system.

a narrow gap where a sample was placed to measure τ_{eff} . Continuous wave (CW) 635 and 980 nm laser diode (LD) lights were introduced to the waveguide tubes. The light intensities were set at 1.5 and 0.98 mW/cm² on the sample surface for 635 and 980 nm lights, respectively, to realize the same photon flux between the two different wavelength lights. The microwave transmission was detected and analyzed to obtain τ_{eff} in the case of light illumination to the top surface (ion-implanted surface), $\tau_{\text{eff}}(\text{top})$, and in the case of light illumination to the rear surface, $\tau_{\text{eff}}(\text{rear})$. The measurement system had a high dynamic τ_{eff} range in the time range from 10⁻⁷ to 10⁻² s. The penetration depth for 635 nm light was about 3 μm , while that for 980 nm light was 125 μm .²³⁾ We constructed a finite-element numerical calculation program including theories of carrier generation associated with optical absorption coefficients, carrier diffusion, and annihilation for estimating the surface recombination velocity on the top surface S_{top} and rear surface S_{rear} and the distribution of the bulk lifetime $\tau_b(x)$ in the depth direction x from the experimental results.¹⁵⁾ The photo induced minority carriers diffuse into the substrate, when CW light is illuminated as²⁴⁾

$$D \frac{\partial^2 n(x)}{\partial x^2} - \frac{n(x)}{\tau_b(x)} + g(x) = 0, \quad (1)$$

where $n(x)$, $g(x)$, and D are the carrier volume density, the carrier generation rate at a depth of x , and the diffusion constant of minority carriers, respectively. Carrier generation occurs in the substrate bulk, which depends on the optical absorption coefficient at a certain light wavelength. Carrier annihilation occurs with $\tau_b(x)$. When the top surface was illuminated with light, the boundary conditions of carrier generation and carrier recombination ratios are given as

$$D \frac{\partial n(x)}{\partial x} \Big|_{x=0} = S_{\text{top}} n(0) - g(0) \Delta x, \quad (2a)$$

$$D \frac{\partial n(x)}{\partial x} \Big|_{x=d} = -S_{\text{rear}} n(d) - g(d) \Delta x, \quad (2b)$$

where d is the thickness of the semiconductor substrate, and Δx is the unit lattice length of the present calculation. In the case of rear surface illumination, S_{top} and S_{rear} exchanged each other in Eqs. (2a) and (2b). Total carrier generation ratio (G) per unit area determined by photon flux and light

reflection loss is given by integrating $g(x)$ with respect to the depth as

$$G = \int_0^d g(x) dx. \quad (3)$$

The most possible S_{top} , S_{rear} , and $\tau_b(x)$ were determined by the best coincidence between the experimental and calculated τ_{eff} values. We also measured the $\tau_{\text{eff}}(\text{top})$ and $\tau_{\text{eff}}(\text{rear})$ of control sample *A* using another method of microwave absorption by carriers generated by multiply periodic pulsed illumination for lifetime calibration.²⁵⁾ This method determines τ_{eff} independently of light intensity, although the measurement accuracy of τ_{eff} is 20 μs .

Optical reflectivity spectra were measured between 250 and 800 nm using a conventional spectrometer to investigate the crystalline volume ratio X in the ion-implanted surface region. They were analyzed using a numerical calculation program, which was constructed with the optical interference effect for an air/SiO₂/multiple-Si layers/Si-substrate structure.^{26,27)} The optical reflectivity on the silicon surface depends on the complex refractive indexes of Si. Using the effective dielectric model, the complex refractive index \tilde{n}_f with the crystalline volume ratio X is determined by combing the crystalline refractive index \tilde{n}_c ²⁸⁾ with the amorphous refractive index \tilde{n}_a ²⁹⁾ as

$$\tilde{n}_f = X\tilde{n}_c + (1 - X)\tilde{n}_a. \quad (4)$$

The thickness and crystalline volume ratio were changed for each layer to calculate the reflectivity. The most possible in-depth distribution of the crystalline volume ratio was obtained by fitting the calculated reflectivity spectra to the experimental reflectivity spectra.

Part of the SiO₂ layer on the rear surface was then removed by hydrofluoric acid for samples *A*, *B*, *C*, and *C*_{anneal}. Al metal electrodes were formed on the top and bear rear surfaces by vacuum evaporation to form the metal oxide semiconductor structure. The capacitance response at an alternative voltage of 1 MHz with an amplitude of 10 mV as a function of the bias voltage ($C-V$) was measured in the dark field to estimate the densities of fixed charges and charge traps at the SiO₂/Si interfaces.³⁰⁾

3. Results and discussion

Figure 2 shows the experimental and calculated optical reflectivity spectra of the initial sample *A* (a), Ge-ion-implanted sample *B* (b), and subsequent-RTA-annealed sample *C* (c). Two large peaks of E_1 and E_2 caused by the large joint density of states at the X point in the Brillouin zone of crystalline silicon appeared at 340 and 275 nm for the initial sample *A*. Decreases in the heights of peaks indicate the partial amorphization of the surface region for the Ge-implanted sample, as shown in Fig. 2(b). On the other hand, RTA heat treatment made the optical reflectivity spectrum almost the same as that of the initial sample, as shown in Fig. 2(c). The best fitting analysis of the calculated optical reflectivity spectra to the experimental ones revealed that the Ge ion implantation slightly dredsuces X in the top 157 nm surface region, as shown in Fig. 3. Although the dose was low at $1 \times 10^{13} \text{ cm}^{-2}$, heavy Ge ions damaged the silicon crystalline lattice. In particular, X decreased to 0.76 in the top 15 nm region from the silicon surface. In the deep region

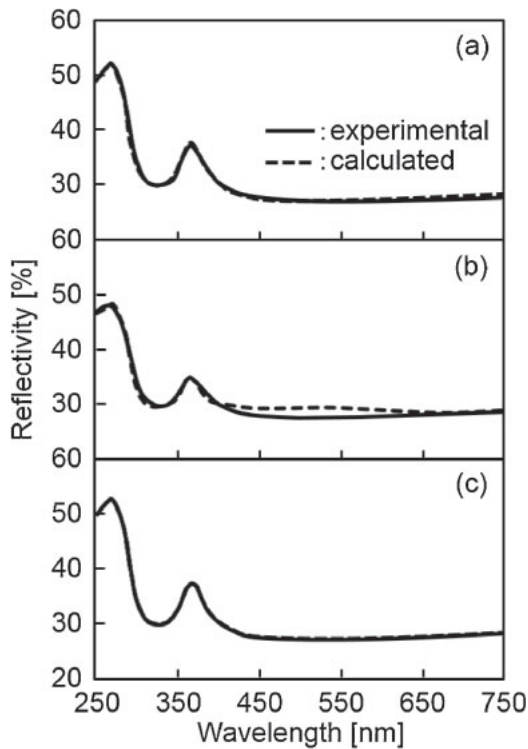


Fig. 2. Experimental and calculated optical reflectivity spectra of the initial sample *A* (a), Ge-ion-implanted sample *B* (b), and subsequent-RTA-annealed sample *C* (c).

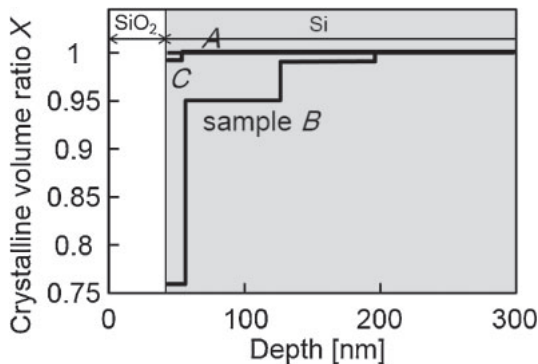


Fig. 3. In-depth profile of the crystalline volume ratio obtained from Fig. 2.

from 15 to 157 nm, X ranged from 0.95 to 0.99. On the other hand, RTA markedly restored X to almost 1 in that surface region. This indicates that RTA recrystallized the region disordered well by Ge ion implantation. The present RTA condition was sufficient for the activation of the implanted species.

Figure 4 shows $\tau_{\text{eff}}(\text{top})$ and $\tau_{\text{eff}}(\text{rear})$ measured by light illumination at (a) 635 nm and (b) 980 nm for samples *A*, *B*, *C*, and *D*. Open and solid circles present $\tau_{\text{eff}}(\text{top})$ and $\tau_{\text{eff}}(\text{rear})$ in the case of 635 nm light illumination, and open and solid triangles present $\tau_{\text{eff}}(\text{top})$ and $\tau_{\text{eff}}(\text{rear})$ in the case of 980 nm light illumination. $\tau_{\text{eff}}(\text{top})$ was high at 2.6×10^{-4} s and the same as $\tau_{\text{eff}}(\text{rear})$ for the initial control sample *A*, as shown in Fig. 4(a). The silicon surfaces were well passivated by the thermally grown SiO_2 layers. Ge ion

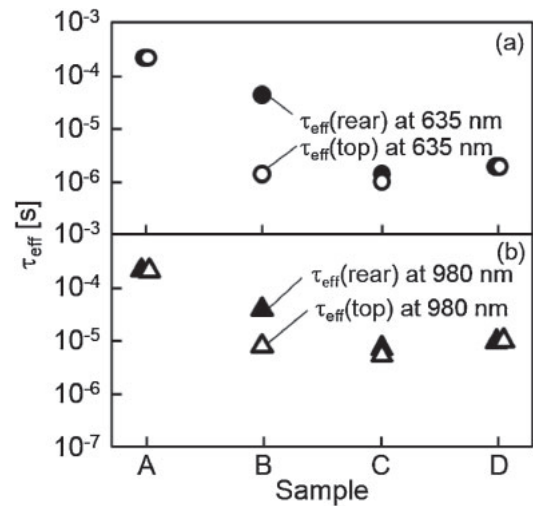


Fig. 4. $\tau_{\text{eff}}(\text{top})$ and $\tau_{\text{eff}}(\text{rear})$ measured by light illumination at (a) 635 nm and (b) 980 nm for samples *A*, *B*, *C*, and *D*.

implantation decreased $\tau_{\text{eff}}(\text{top})$ and $\tau_{\text{eff}}(\text{rear})$. In particular, $\tau_{\text{eff}}(\text{top})$ markedly decreased to 1.6×10^{-6} s because Ge ion implantation caused serious damage, increasing the carrier recombination probability on the surface, as shown by sample *B* in Fig. 4(a). $\tau_{\text{eff}}(\text{rear})$ was 4.9×10^{-5} s, which was higher than $\tau_{\text{eff}}(\text{top})$. This indicates that photoinduced carriers generated on the rear surfaces survived during diffusion in the silicon substrate and then annihilated on the top surface. The subsequent RTA shows small $\tau_{\text{eff}}(\text{top})$ and $\tau_{\text{eff}}(\text{rear})$ values of 1.1×10^{-6} and 1.6×10^{-6} s for sample *C*, as shown in Fig. 4(a), in spite of the complete recrystallization in the implanted surface region by RTA, as shown in Fig. 4(a). Such small $\tau_{\text{eff}}(\text{top})$ and $\tau_{\text{eff}}(\text{rear})$ values suggest that RTA generated a number of substantial minority carrier recombination defects in silicon. To demonstrate the effect of RTA on τ_{eff} , the initial sample was treated only with RTA. $\tau_{\text{eff}}(\text{top})$ and $\tau_{\text{eff}}(\text{rear})$ were markedly reduced to 2.2×10^{-6} s by RTA, as shown by sample *D* in Fig. 4(a). This explicitly shows that RTA generated a substantial number of carrier recombination defects in silicon substrate.

Large $\tau_{\text{eff}}(\text{top})$ and $\tau_{\text{eff}}(\text{rear})$ values of 2.8×10^{-4} s were also observed for the control sample *A* in the case of 980 nm light illumination, as shown in Fig. 4(b). They were slightly higher than those in the case of 635 nm light illumination. This indicates that the density of carrier recombination sites was low and concentrated at the SiO_2/Si interfaces. Ge ion implantation decreased $\tau_{\text{eff}}(\text{top})$ and $\tau_{\text{eff}}(\text{rear})$ to 9.5×10^{-6} and 4.4×10^{-5} s, respectively, in the case of 980 nm light illumination. These $\tau_{\text{eff}}(\text{top})$ and $\tau_{\text{eff}}(\text{rear})$ values were larger and smaller than those, respectively. The small $\tau_{\text{eff}}(\text{rear})$ value in the case of 980 nm light illumination suggests that carrier recombination sites were formed in a very deep region from the top surface. The carriers generated up to a 125- μm -deep rear surface region rapidly reached the carrier recombination sites in the top surface region reducing $\tau_{\text{eff}}(\text{rear})$ in the case of 980 nm light illumination. The subsequent RTA resulted in small $\tau_{\text{eff}}(\text{top})$ and $\tau_{\text{eff}}(\text{rear})$ values of 5.6×10^{-6} and 8.0×10^{-6} s, as shown in Fig. 4(b). They were higher than those in the case of 635 nm light illumination. Such results indicate that carrier annihilation sites localized in both

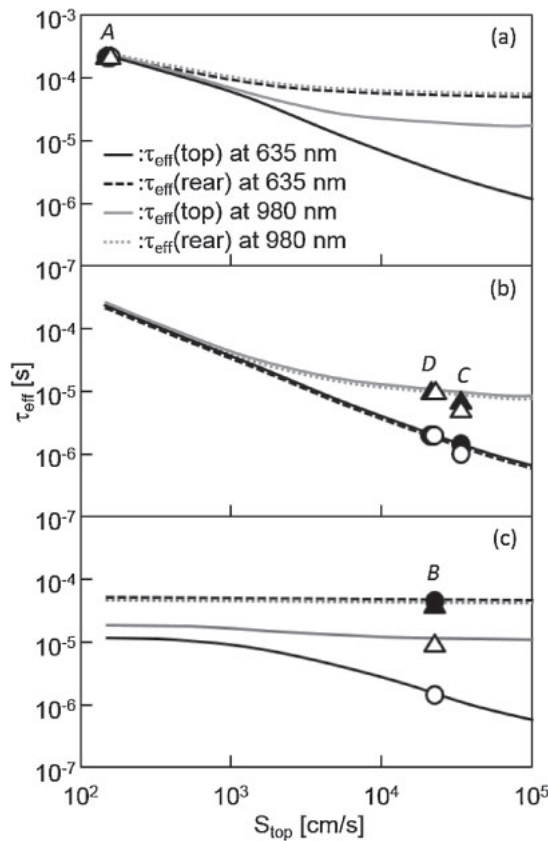


Fig. 5. Numerically calculated $\tau_{\text{eff}}(\text{top})$ and $\tau_{\text{eff}}(\text{rear})$ in the cases of 635 and 980 nm light illuminations as a function of S_{top} assumed (a) with a sufficiently high τ_b of 2.0×10^{-2} s in the entire thickness range and a constant S_{rear} of 132 cm/s, (b) with a high τ_b of 2.0×10^{-2} s in the entire thickness range and $S_{\text{rear}} = S_{\text{top}}$, and (c) with τ_b of 5.0×10^{-6} s from the top 200 μm region and of 2.0×10^{-2} s from the depth of 200 μm to the bottom surface, and S_{rear} of 132 cm/s. Experimental data were also obtained under the best agreement conditions.

surface regions. The sole RTA treatment decreased $\tau_{\text{eff}}(\text{top})$ and $\tau_{\text{eff}}(\text{rear})$ to about 1.1×10^{-5} s in the case of 980 nm light illumination, as shown by sample *D* in Fig. 4(b).

The $\tau_{\text{eff}}(\text{top})$ and $\tau_{\text{eff}}(\text{rear})$ values shown in Fig. 4 were analyzed using our finite element program to estimate S_{top} , S_{rear} , and $\tau_b(x)$. Fitting the calculated $\tau_{\text{eff}}(\text{top})$ and $\tau_{\text{eff}}(\text{rear})$ values to experimental ones was conducted with different sets of S_{top} , S_{rear} , and $\tau_b(x)$. Their best coincidence gave the most possible S_{top} , S_{rear} , and $\tau_b(x)$. τ_b for the control sample *A* was assumed to be sufficiently high at 2.0×10^{-2} s. S_{rear} in the case of the as-Ge-implanted sample *B* was assumed to be the same as that of sample *A*. Figure 5 shows the results of the fitting process, namely, the numerical calculated $\tau_{\text{eff}}(\text{top})$ and $\tau_{\text{eff}}(\text{rear})$ values in the cases of 635 and 980 nm light illuminations as a function of S_{top} assumed (a) with a τ_b of 2.0×10^{-2} s in the entire thickness range and a S_{rear} of 132 cm/s, (b) with a high τ_b of 2.0×10^{-2} s in the entire thickness range and $S_{\text{rear}} = S_{\text{top}}$, and (c) with a τ_b of 5.0×10^{-6} s from the top 200 μm region and a τ_b of 2.0×10^{-2} s from the depth of 200 μm to the bottom surface, and S_{rear} of 132 cm/s. The experimental τ_{eff} values shown in Fig. 4 were obtained under the best coincident conditions. The experimental τ_{eff} values for samples *A*, *C* and *D*, and *B* are given in Figs. 5(a)–5(c). All τ_{eff} values decreased when S_{top} increased in three different

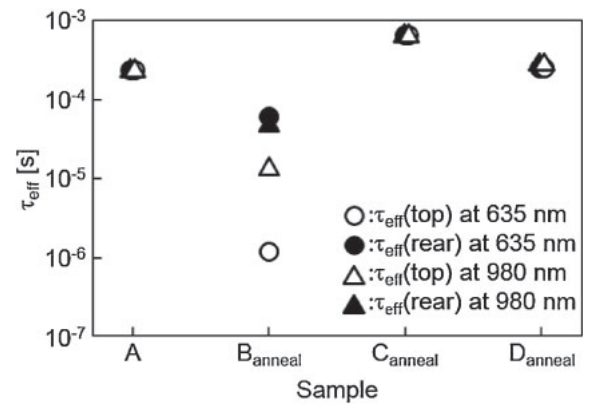


Fig. 6. $\tau_{\text{eff}}(\text{top})$ and $\tau_{\text{eff}}(\text{rear})$ measured by light illumination at 635 and 980 nm for samples *B_{anneal}*, *C_{anneal}*, and *D_{anneal}* annealed by 1.3×10^6 Pa H_2O vapor heat treatment at 260 $^\circ\text{C}$ for 3 h.

defect distribution cases. Figure 5(a) shows that $\tau_{\text{eff}}(\text{top})$ and $\tau_{\text{eff}}(\text{rear})$ in the case of 980 nm light illumination are higher than those in the case of 635 nm light illumination for the high S_{top} conditions because the carriers generated in deep regions by 980 nm light show a large τ_{eff} value owing to the duration diffusion to the top surface. $\tau_{\text{eff}}(\text{top})$ equals $\tau_{\text{eff}}(\text{rear})$ in the cases of 635 and 980 nm light illuminations because of the symmetrical defect distribution $S_{\text{top}} = S_{\text{rear}}$, as shown in Fig. 5(b). On the other hand, the introduction of the small τ_b value of 5.0×10^{-6} s in the top 200 μm surface region markedly decreased $\tau_{\text{eff}}(\text{top})$ in the cases of 635 and 980 nm light illuminations, as shown in Fig. 5(c). $\tau_{\text{eff}}(\text{top})$ for 980 nm light illumination and $\tau_{\text{eff}}(\text{rear})$ for 635 and 980 nm light illuminations had no marked dependence on S_{top} . Such results are due to the carriers generated in the region with high τ_b (from 200 μm deep region to the bottom surface) being mainly annihilated by diffusion to the low τ_b region. Although the Ge-implanted region was limited only in the 157 nm surface region, the analysis revealed that the top 200 μm deep surface region had a small τ_b value of 5.0×10^{-6} s probably because of heavy Ge ion damage, as shown in Fig. 5(c). The same high surface carrier recombination velocities ($S_{\text{top}} = S_{\text{rear}}$) of 3.0×10^4 and 2.0×10^4 cm/s were obtained for the two RTA-treated samples *C* (Ge implanted) and *D*, respectively, as shown in Fig. 5(b). RTA generated a high density of carrier recombination sites on the top and rear surfaces. A substantial number of recombination defect states were probably generated in the silicon surface region during and after RTA. The decreased SiO_2 passivation effect could also increase the surface recombination velocity. The stable bonding configuration established at the thermally grown SiO_2/Si interface would have been changed by a high thermal stress owing to the difference in thermal expansion coefficient between SiO_2 and Si.

Figure 6 shows $\tau_{\text{eff}}(\text{top})$ and $\tau_{\text{eff}}(\text{rear})$ measured by light illumination at 635 and 980 nm for samples *B_{anneal}*, *C_{anneal}*, and *D_{anneal}* annealed by 1.3×10^6 Pa H_2O vapor heat treatment at 260 $^\circ\text{C}$ for 3 h. Open and solid circles indicate $\tau_{\text{eff}}(\text{top})$ and $\tau_{\text{eff}}(\text{rear})$ in the case of 635 nm light illumination, and open and solid triangles indicate $\tau_{\text{eff}}(\text{top})$ and $\tau_{\text{eff}}(\text{rear})$ in the case of 980 nm light illumination. $\tau_{\text{eff}}(\text{top})$ and $\tau_{\text{eff}}(\text{rear})$ for the initial sample *A* are also plotted for comparison. The

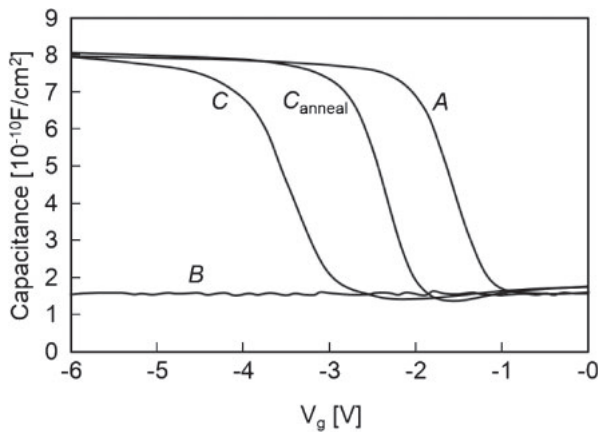


Fig. 7. Capacitance response as a function of bias voltage with 1 MHz alternative voltage for the initial sample *A*, as-Ge implanted sample *B*, Ge-implanted and then RTA-treated sample *C*, and sample *C_{anneal}* subsequently heat treated with H₂O vapor at 1.3×10^6 Pa.

H₂O vapor heat treatment hardly changed the $\tau_{\text{eff}}(\text{top})$ and $\tau_{\text{eff}}(\text{rear})$ of the as-Ge-implanted sample in the cases of 635 and 980 nm light illuminations, as shown by sample *B_{anneal}*. This indicates that the Ge-implanted surface region had a residually high density of carrier recombination defect states after H₂O vapor heat treatment. The crystalline volume ratio was not improved by the H₂O vapor heat treatment. On the other hand, the H₂O vapor heat treatment markedly increased the $\tau_{\text{eff}}(\text{top})$ and $\tau_{\text{eff}}(\text{rear})$ of the as-Ge-implanted followed by RTA treated sample between 6.5×10^{-4} and 6.9×10^{-4} s in the cases of 635 and 980 nm light illuminations, as shown by sample *C_{anneal}*. Such a treatment also increased the $\tau_{\text{eff}}(\text{top})$ and $\tau_{\text{eff}}(\text{rear})$ of the sole-RTA-treated sample between 2.6×10^{-4} and 2.9×10^{-4} s in the cases of 635 and 980 nm light illuminations, as shown by sample *D_{anneal}*. Such results clearly show that H₂O vapor postannealing at 260 °C cured the carrier recombination defect states on the silicon surfaces generated by RTA or made the SiO₂/Si interface stable. The carrier recombination velocity was decreased from 132 to 60 cm/s. Thus post-low-temperature annealing is important for high-temperature RTA thermal treatment.

Figure 7 shows *C*-*V* characteristics of the initial sample *A*, as-Ge implanted sample *B*, Ge-implanted followed by RTA treated sample *C*, and sample *C_{anneal}* annealed by subsequent 1.3×10^6 Pa H₂O vapor heat treatment. A sharp change in capacitance was observed for the initial sample *A*. It indicates that the sample had a low density of interface traps. The analysis with the high-frequency capacitance response resulted in densities of interface traps at the mid-gap and fixed charges of 8.5×10^{10} eV⁻¹ cm⁻² and 4.3×10^{11} cm⁻², respectively. On the other hand, no capacitance change was observed in the case of the as-Ge-implanted sample *B*. The high densities of interface traps and fixed charges generated by Ge implantation did not allow a change in the surface potential in the measurement range. The subsequent RTA treatment succeeded in changing the capacitance, as shown by sample *C* in Fig. 7. However, the slope of the capacitance change was gentle compared with that of sample *A*. Moreover, the substantially shifted *C*-*V* curve in the negative voltage direction. The analysis with the high-frequency capacitance response resulted in densities of interface traps

at the mid-gap and fixed charges of 9.1×10^{11} eV⁻¹ cm⁻² and 1.1×10^{12} cm⁻², respectively. The high density of interface traps probably resulted in the small τ_{eff} and high *S* values, as shown in Figs. 4 and 5. On the other hand, the 1.3×10^6 Pa H₂O vapor heat treatment induced a sharp change in capacitance, although *C*-*V* curve still shifted in the negative voltage direction. The analysis with the high-frequency capacitance response resulted in densities of interface traps at the mid-gap and fixed charges of 3.6×10^{10} eV⁻¹ cm⁻² and 7.5×10^{11} cm⁻², respectively. The marked decrease in the density of interface traps probably succeeded in increasing τ_{eff} and decreasing *S*. Moreover, the high density of residual fixed charge would have induced the inversion mode with a high density of electron carriers on the surface under the free potential condition. Although photo-induced minority electron carriers must be promoted to move the surface by the potential slope formed by the fixed charges,²⁴⁾ the high density of electrons accumulating in the surface region probably suppressed the carrier recombination.

The investigation of photoinduced minority carrier lifetime, carrier recombination velocity, and *C*-*V* characteristics revealed that RTA was not a sufficient heat treatment. Rapid heating to a high temperature leaves defective states with a high carrier recombination defect density generated at SiO₂/Si interfaces. Thus low-temperature postannealing at is important in improving minority carrier properties.

4. Conclusions

We measured changes in the τ_{eff} of p-type 700- μm -thick silicon substrates coated with 43-nm-thick thermally grown SiO₂ layers by Ge ion implantation at a dose of 1×10^{13} cm⁻² at 150 keV and RTA at 1100 °C for 50 s. We used a highly sensitive measurement system for τ_{eff} under CW light illumination at 635 and 980 nm. Ge ion implantation decreased the crystalline volume ratio to 0.76 in the surface region. The crystalline volume ratio was lower than 1.0 in the top 157 nm region. Ge ion implantation markedly decreased $\tau_{\text{eff}}(\text{top})$ to 1.6×10^{-6} s in the case of 635 nm light illumination. $\tau_{\text{eff}}(\text{top})$ was also small at 9.5×10^{-6} s in the case of 980 nm light illumination. The analysis of the experimental results revealed that Ge implantation caused a high *S_{top}* value of 2.0×10^4 cm/s and a small τ_b value of 5.0×10^{-6} s in the top 200 μm surface region. Although RTA successfully induced the recrystallization of the surface region damaged by ion implantation, it markedly decreased $\tau_{\text{eff}}(\text{top})$ and $\tau_{\text{eff}}(\text{rear})$ to 1.1×10^{-6} and 1.6×10^{-6} s, respectively, in the case of 635 nm light illumination. The small $\tau_{\text{eff}}(\text{top})$ and $\tau_{\text{eff}}(\text{rear})$ values indicate that RTA caused a substantial thermal stress associated with a high surface recombination velocity of 3.0×10^4 cm/s. $\tau_{\text{eff}}(\text{top})$ and $\tau_{\text{eff}}(\text{rear})$ were also decreased to 2.2×10^{-6} s by RTA alone. The measurement of *C*-*V* characteristics revealed that RTA resulted in a high density of interface traps of 9.1×10^{11} eV⁻¹ cm⁻². The subsequent 1.3×10^6 Pa H₂O vapor heat treatment at 260 °C for 3 h markedly increased $\tau_{\text{eff}}(\text{top})$ and $\tau_{\text{eff}}(\text{rear})$ between 6.5×10^{-4} and 6.9×10^{-4} s. Thus, post-low-temperature annealing is effective in curing the recombination defect states generated by RTA. The interface trap density was decreased to 3.6×10^{10} eV⁻¹ cm⁻², indicating that post annealing is very important in reducing the density of minority carrier sensitive defects in the RTA process.

Acknowledgment

We thank Sameken Co., Ltd. for the support.

- 1) M. Mehrotra, J. C. Hu, A. Jain, W. Shiau, V. Reddy, S. Aur, and M. Rodder, *IEDM Tech. Dig.*, 1999, p. 419.
- 2) T. Ito, K. Suguro, M. Tamura, T. Taniguchi, Y. Ushiku, T. Inuma, T. Itani, M. Yoshioka, T. Owada, Y. Imaoka, H. Murayama, and T. Kusuda, *Ext. Abstr. 3rd Int. Workshop Junction Technology*, 2002, p. 23.
- 3) A. Shima and A. Hiraiwa, *Jpn. J. Appl. Phys.* **45**, 5708 (2006).
- 4) K. Goto, T. Yamamoto, T. Kubo, M. Kase, Y. Wang, T. Lin, S. Talwar, and T. Sugii, *IEDM Tech. Dig.*, 1999, p. 931.
- 5) S. M. Sze, *Semiconductor Devices* (Wiley, New York, 1985) Chap 7.
- 6) E. A. G. Webster, L. A. Grant, and R. K. Henderson, *IEEE Trans. Electron Devices* **60**, 1188 (2013).
- 7) S. E. Bohndiek, C. D. Arvanitis, G. J. Royle, A. T. Clark, J. P. Crooks, M. L. Prydderch, R. Turchetta, A. Blue, V. O'Shea, and R. D. Speller, *Opt. Eng.* **46**, 124003 (2007).
- 8) E. A. G. Webster, L. A. Grant, and R. K. Henderson, *IEEE Electron Device Lett.* **33**, 1589 (2012).
- 9) C. D. Arvanitis, S. E. Bohndiek, G. J. Royle, A. Blue, H. X. Liang, A. Clark, M. Prydderch, R. Turchetta, and R. D. Speller, *Med. Phys.* **34**, 4612 (2007).
- 10) A. Rohatagi, Proc. 3rd World Conf. Photovoltaic Energy Conversion, 2003, A29.
- 11) M. A. Green, *Prog. Photovoltaics* **17**, 183 (2009).
- 12) M. A. Green, K. Emery, Y. Hishikawa, W. Warta, and E. D. Dunlop, *Prog. Photovoltaics* **20**, 12 (2012).
- 13) J. Zhao, A. Wang, M. A. Green, and F. Ferrazza, *Appl. Phys. Lett.* **73**, 1991 (1998).
- 14) T. Sameshima, K. Betsuin, T. Mizuno, and N. Sano, *Jpn. J. Appl. Phys.* **51**, 03CA04 (2012).
- 15) T. Sameshima, R. Ebina, K. Betsuin, Y. Takiguchi, and M. Hasumi, *Jpn. J. Appl. Phys.* **52**, 011801 (2013).
- 16) H. H. Andersen and J. F. Ziegler, *Stopping and Ranges of Ions in Matter* (Pergamon, New York, 1977) Vol. 3.
- 17) T. Sameshima and M. Satoh, *Jpn. J. Appl. Phys.* **36**, L687 (1997).
- 18) T. Sameshima, M. Satoh, K. Sakamoto, K. Ozaki, and K. Saitoh, *Jpn. J. Appl. Phys.* **37**, 4254 (1998).
- 19) K. Sakamoto and T. Sameshima, *Jpn. J. Appl. Phys.* **39**, 2492 (2000).
- 20) H. Watakabe, T. Sameshima, T. Strutz, T. Oitome, and A. Kohno, *Jpn. J. Appl. Phys.* **44**, 8367 (2005).
- 21) T. Sameshima, H. Hayasaka, and T. Haba, *Jpn. J. Appl. Phys.* **48**, 021204 (2009).
- 22) T. Sameshima, T. Nagao, M. Hasumi, A. Shuku, E. Takahashi, and Y. Andoh, *Jpn. J. Appl. Phys.* **51**, 03CA06 (2012).
- 23) E. D. Palk, *Handbook of Optical Constants of Solids* (Academic Press, London, 1985) p. 547.
- 24) A. S. Groove, *Physics and Technology of Semiconductor Devices* (Wiley, New York, 1967) Chap. 5.
- 25) T. Sameshima, T. Nagao, S. Yoshidomi, K. Kogure, and M. Hasumi, *Jpn. J. Appl. Phys.* **50**, 03CA02 (2011).
- 26) T. Sameshima, Y. Matsuda, Y. Andoh, and N. Sano, *Jpn. J. Appl. Phys.* **47**, 1871 (2008).
- 27) M. Born and E. Wolf, *Principles of Optics* (Pergamon, New York, 1974) Chaps. 1 and 13.
- 28) E. D. Palk, *Handbook of Optical Constants of Solids* (Academic Press, London, 1985) pp. 562 and 577.
- 29) J. R. Chelikowsky and M. L. Cohen, *Phys. Rev. B* **10**, 5095 (1974).
- 30) Y. Taur and T. Ning, *Fundamental of Modern VLSI Physics* (Cambridge University Press, Cambridge, U.K., 1998) Chap. 2.